The Effect of P_2O_5 on the Crystallization Behaviors of Ti-Bearing Blast Furnace Slags Using Single Hot Thermocouple Technique

YONGQI SUN, JING LI, XIDONG WANG, and ZUOTAI ZHANG

The present paper investigates how the P_2O_5 addition influences the crystallization behaviors of Ti-bearing blast furnace (Ti-BF) slags with different basicity using Single Hot Thermocouple Technique. It was found that the basicity showed a significant effect on the crystallization behaviors of the Ti-BF slags, and the trend of formation of the rod-shape crystal decreased while the trend of formation of dendrite crystal increased with increasing basicity. The addition of P_2O_5 was found to promote the formation of rod-shape crystal. The basicity and crystallization temperature that the rod-shape crystal could be formed increased, while the incubation time of formation of the rod-shape crystal decreased with increasing P_2O_5 content. Scanning electron microscope equipped with energy-dispersive X-ray spectroscope and X-ray diffraction were employed to observe the morphology and determine the crystalline phase of the Ti-enriched crystals. The results indicated that the rod-shape crystal was rutile. The kinetics of the formation of rutile was studied, and the mechanism of crystallization and growth was further discussed. The results indicated that the crystallization of rutile was one-dimensional interface-controlled growth, and the nucleation rate varied with the holding time.

DOI: 10.1007/s11663-014-0077-0

I. INTRODUCTION

CHINA'S titanium resource is quite abundant, which ranks first in the world, and the vanadium titanium-magnetite ore in Panzhihua city, Sichuan province in China accounts for 91 pct.[1] At the present time, blast furnace processing is the main method used to extract valuable elements (*e.g.*, Fe and V) from the vanadium titanium-magnetite ores and titanium element comes into blast furnace slags, which forms typical Ti-bearing blast furnace slags (Ti-BF slags). China has accumulated more than 70 million tons of Ti-BF slags, and it is still increasing by 3 million tons per year.[2] The Ti-BF slags generally contain 22 to 25 wt pct TiO_2,[3] and it has been thought to be an important secondary resource for titanium-extracting process. Up to now, there are four major alternative methods proposed to extract titanium from the Ti-BF slags, acid leaching method,[4,5] alkaline molten salt method,[6,7] high-temperature carbonization method,[8,9] and selective crystallization and phase separation (SCPS) method.[10,11] These methods show some advantages and disadvantages, respectively. Acid leaching and alkaline molten salt methods may cause serious pollution, while high-temperature carbonization method consumes large quantities of energy. SCPS method has been thought as a potential method, and the selective crystallization is the key step to successfully extract titanium. Many researchers have carried out experiments to study the selective crystallization behaviors of perovskite.[10,11] However, it has been proved that the perovskite shows poor separation property because of its dendrite structure and similar density with other phases.[12] Other crystalline phases such as rutile were thought to be potential selective phases, which has the rod-shape structure and a higher density (4.2 to 4.3 g/cm^3). Li *et al.*[13–15] studied the selective crystallization behaviors of rutile in the Ti-BF slags.The crystallization behaviors of rutile have been investigated in the Ti-BF slags, which were modified through the addition of SiO_2, and it was found that the optimum content of SiO_2 was 35 pct and the basicity was 0.5, *i.e.*, a large amount of SiO_2 being used to modify the Ti-BF slags was required to form rutile. The present research was, therefore, motivated to decrease the SiO_2 content during modification of the Ti-BF slags through adding a small amount of P_2O_5, and it is expected that small amount of P_2O_5 addition can obviously decrease the addition of SiO_2 during the basicity modification of the slags.

YONGQI SUN, Doctoral Candidate, is with the Department of Energy and Resource Engineering, College of Engineering, Peking University, Beijing 100871, P.R. China. JING LI, formerly Ph.D. Candidate with the Department of Energy and Resource Engineering, College of Engineering, Peking University, is now Engineer with the Aluminum Corporation of China, Beijing 100082, P.R. China. XIDONG WANG and ZUOTAI ZHANG, Professors, are with the Department of Energy and Resource Engineering, College of Engineering, Peking University, and also with the Beijing Key Laboratory for Solid Waste Utilization and Management, Peking University, Beijing 100871, P.R. China. Contact e-mail: zuotaizhang@pku.edu.cn
Manuscript submitted June 29, 2013.
Article published online April 29, 2014.

II. EXPERIMENTAL

A. *Sample Preparation*

In the present experiments, the modified slags were prepared using analytically pure (AR) CaO, MgO, SiO_2,

TiO_2, Al_2O_3, and P_2O_5. There were 3 slag series (shown as A, B, and C) studied in this study. The compositions of designed samples are listed in Table I, and the P_2O_5 content increases from 0 to 7 pct at different basicities. Then, the mixture in a molybdenum crucible ($\Phi 40 \times 45 \times H40$ mm) was melted under an argon atmosphere at 1773 K (1500 °C) for 2 hours to homogenize its chemical composition; after that, the liquid slags were rapidly poured into cool water to obtain the glassy slags. The XRD analyses proved that the quenched slags showed glassy phase. Subsequently, the glassy slags were dried at 393 K (120 °C) for 12 hours, crushed, and grinded to 300 meshes for the single hot thermocouple technique (SHTT) tests. The pre-melted slags were analyzed by X-ray fluoroscopy (XRF), as listed in Table I. It can be seen that the XRF values showed a small deviation compared with the designed composition.

B. *Experimental Procedures*

Experiments were carried out using SHTT, which has been approved to be an effective method to investigate the crystallization behaviors in the melts in the previous papers,[16–22] and the working mechanism will be briefly introduced here. A Pt–Rh thermocouple was used to heat or cool the sample and measure the temperature simultaneously, and the heating and cooling processes were controlled by a computer program. The images of melts were captured by a microscope equipped with a video camera and then sent to the computer and used to analyze the crystallization behaviors. During the experiments, a small amount of sample (about 10 mg) was mounted on the tip of thermocouple, heated to 1773 K (1500 °C), and held for 120 seconds in order to eliminate the bubbles and homogenize the chemical composition. After that, the sample was rapidly cooled (50 K/s) to a given temperature and held for 300 to 1800 seconds. The sample images were recorded, and based on the image analysis, the time for the beginning of crystallization was determined; time–temperature-transformation (TTT) diagrams were, therefore, constructed, and the kinetics study could be, therefore, investigated. In order to reduce the experimental error, each new thermocouple was used during the construction of TTT diagrams. X-ray powder diffraction (XRD) analysis was used to identify the crystalline phase of the modified Ti-BF slags. Scanning electron microscope (SEM) was carried out and back-scattered electron (BSE) images were obtained in order to observe the microstructure of the samples and identify the chemical composition of the crystal with energy-dispersive X-ray spectroscopy (EDX). The post-SHTT experiment sample size was sufficiently small that it could not be characterized through XRD. Therefore, in order to determine the crystalline phase, larger pre-melted glassy slag samples were heat-treated in a resistance furnace at different temperatures and quenched in water. The samples obtained this way were examined at room temperature by XRD technique.

III. RESULTS AND DISCUSSION

A. *TTT Diagrams*

To construct TTT diagrams, isothermal experiments were carried out using SHTT in a temperature range of 1173 K to 1673 K (900 °C to 1400 °C) in the present experiments, and each point in TTT diagrams is an average value of three observations. Figure 1 shows the TTT diagrams of modified slags.It could be observed that these curves showed double noses except samples A5 and B5 and that the crystallization occurred during the cooling process, which indicated that there were two different nucleation events in the crystallization process that the crystalline morphology or crystalline phases drastically changed. The crystallization temperature of the rod-shape crystal is shown in Figure 2, and it can be seen that the crystallization temperature increased with increasing P_2O_5 content. For slag series A, two different crystal morphologies, the rod shape and cloud shape, were observed at different temperatures. Figure 3 shows the morphology change of crystal precipitated from 1513 K, 1393 K, and 1313 K (1240 °C, 1120 °C, and 1040 °C) for sample A1, respectively. It can be clearly seen that the crystal showed typical rod-shape and cloud-shape structure as the temperatures are 1513 K and 1313 K (1240 °C and 1040 °C), respectively, and the crystal with cloud and rod shapes appeared simultaneously at 1393 K (1120 °C). With the decrease of temperature, the distribution of nucleation sites changed, as shown in Figure 3. As for slag series B, the dendrite crystal was observed to precipitate for samples B1 and B2 at the whole temperature ranges, and the rod-shape crystal was found to precipitate for samples B3, B4, and B5 when P_2O_5 content was over 3 pct, as shown in Figure 4. As for slag series C, the rod-shape crystal was observed to form in the sample C5 when the temperature is beyond 1333 K (1060 °C), while the morphology of the crystal showed dendrite shape at high temperatures for samples when P_2O_5 was below 7 pct.

From the aforementioned results, it can be found that the basicity and the content of P_2O_5 showed significant influence on the crystallization behaviors of the modified slags. The rod-shape crystal was formed over 1373 K (1100 °C) for sample A1 while the dendrite crystal was formed with increasing basicity over 1293 K (1020 °C) (sample B1) and 1333 K (1060 °C) (sample C1), and no rod-shape crystal was observed for samples B1 and C1. For slag series A, the rod-shape crystal was precipitated even without P_2O_5 addition, while for slag series B and slag series C, the rod-shape crystal appeared only when P_2O_5 was over 3 and 7 pct, respectively, *i.e.*, the addition of P_2O_5 can promote while the basicity suppresses the formation of rod-shape crystal.

The incubation time was another important parameter to characterize the crystallization property, and a shorter incubation time suggested a stronger crystallization trend. Figure 1(b) shows that the incubation time of rod-shape crystal formation decreased in the zone of formation of rod-shape crystal with the increase of P_2O_5 content, indicating that the addition of P_2O_5 is beneficial

Table I. The Chemical Compositions of Modified Ti-BF Slags (in Mass Pct)

Series	Samples	Basicity(B)	CaO	SiO_2	Al_2O_3	MgO	TiO_2	P_2O_5
A	A1							
	Designed	0.50	18.70	37.32	11.97	7.05	24.96	
	XRF	0.56	19.39	34.44	13.29	7.90	24.98	
	A2							
	Designed	0.50	18.53	37.00	11.86	6.93	24.72	0.97
	XRF	0.57	19.31	34.06	12.91	7.75	24.93	1.04
	A3							
	Designed	0.50	18.13	36.25	11.63	6.79	24.27	2.93
	XRF	0.57	18.93	33.49	13.12	7.61	24.08	2.77
	A4							
	Designed	0.50	17.75	35.55	11.42	6.68	23.80	4.80
	XRF	0.56	18.50	33.28	12.84	7.63	23.20	4.56
	A5							
	Designed	0.50	17.32	34.54	11.09	6.48	23.14	7.44
	XRF	0.60	18.76	31.11	12.42	7.69	22.86	7.16
B	B1							
	Designed	0.70	23.08	32.91	12.02	7.00	25.00	
	XRF	0.76	23.52	30.79	13.06	7.69	24.93	
	B2							
	Designed	0.70	22.83	32.61	11.94	6.93	24.71	0.97
	XRF	0.74	22.78	30.97	13.35	7.84	24.10	0.95
	B3							
	Designed	0.70	22.34	32.01	11.62	6.80	24.32	2.91
	XRF	0.77	23.01	30.01	12.57	7.47	24.24	2.69
	B4							
	Designed	0.70	22.00	31.37	11.39	6.69	23.77	4.78
	XRF	0.76	22.56	29.61	12.85	7.60	22.65	4.73
	B5							
	Designed	0.70	21.38	30.47	11.10	6.50	23.14	7.41
	XRF	0.80	22.42	28.00	12.30	7.39	22.82	7.06
C	C1							
	Designed	0.90	26.55	29.47	11.98	6.98	25.03	
	XRF	0.96	26.53	27.69	13.12	7.74	24.92	
	C2							
	Designed	0.90	26.23	29.18	11.93	6.91	24.74	1.01
	XRF	0.92	25.80	27.99	13.32	7.87	23.96	1.07
	C3							
	Designed	0.90	25.75	28.63	11.61	6.76	24.32	2.93
	XRF	0.93	25.60	27.65	12.78	7.55	23.56	2.85
	C4							
	Designed	0.90	25.25	28.04	11.45	6.68	23.78	4.79
	XRF	0.97	25.65	26.36	12.47	7.36	23.45	4.71
	C5							
	Designed	0.90	24.52	27.32	11.11	6.48	23.15	7.41
	XRF	0.95	24.82	26.06	12.18	7.29	22.55	7.10

for the rod-shape crystal formation. The influence of P_2O_5 on the crystallization became more complicated for slag series B. The incubation time of formation of rod-shape crystal became shorter with the increase of P_2O_5 content for samples B3, B4, and B5, while the incubation time of the formation of the dendrite crystal became longer from B1 to B2 as shown in Figure 1(c), which suggested that higher P_2O_5 content contributed to the crystallization of rod-shape crystal and restrained the crystallization of dendrite crystal. As for slag series C, the incubation time of the formation of the dendrite crystal increased with small amount of P_2O_5 addition, and further addition of P_2O_5 showed small effect on the incubation time, as shown in Figure 1(d). It can be seen from the above results that the initial structure of the high-basicity slag melts (samples B1 and C1) limited the formation of the rod-shape crystal. P_2O_5 was a typical network-forming oxide, and it could remarkably change the melts' structure in a direction of enhancing the formation of rod-shape crystal and it has been studied in a previous paper[23] that the addition of P_2O_5 could promote the affinity between phosphorous complex and Ca ions.

In a word, for slag series A, the incubation time of formation of rod-shape crystal became shorter with the addition of P_2O_5, while for slag series B and C, the formation of rod-shape crystal became possible with the addition of P_2O_5. It suggested that P_2O_5 addition is beneficial for the formation of rod-shape crystal and restrained the formation of dendrite crystal.

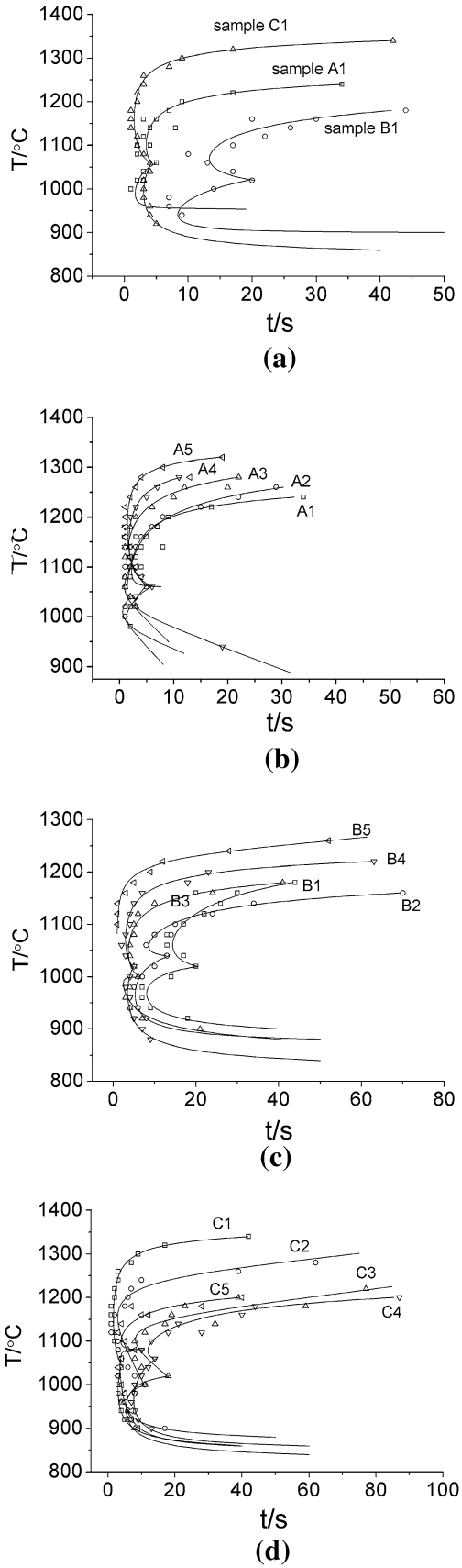

Fig. 1—TTT diagrams of the modified slags (*a*) slags without P_2O_5, (*b*) slag series A, (*c*) slag series B, and (*d*) slag series C.

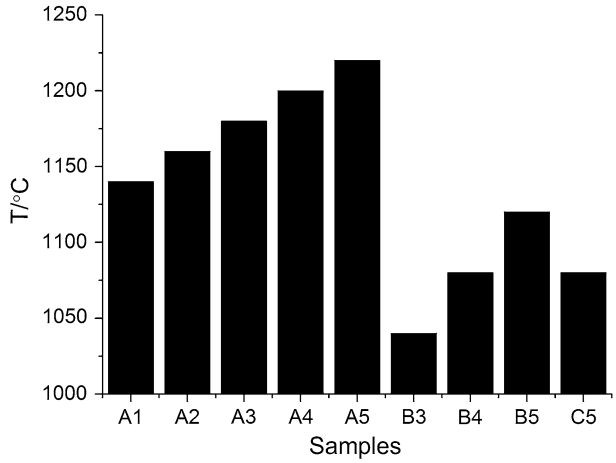

Fig. 2—Crystallization temperatures of rod-shape crystal formation.

B. *Crystalline Phases*

As aforementioned, the rod-shape crystal was found to be formed in 9 samples. The rod-shape crystal was examined using XRD technique, and Figure 5(a) shows the XRD result of sample A1 quenched from 1493 K (1220 °C). It can be seen that the rod-shape crystal was rutile, which was in agreement with a previous study.[13] Figure 5(b) shows the XRD results of the sample A2 quenched from 1533 K, 1393 K, and 1313 K (1260 °C, 1120 °C, and 1040 °C), respectively. As can be seen, rutile was the only crystal precipitating at 1533 K (1260 °C), whereas $CaMgSi_2O_6$, $CaAl_2Si_2O_8$, and $CaTiSiO_5$ were formed when the temperature decreased to 1313 K (1040 °C). Figure 5(c) illustrates the XRD results of sample B1 quenched from 1473 K (1200 °C) and sample B5 quenched from 1493 K (1220 °C), respectively, when the crystalline morphology showed typical dendrite and rod shape. It can be seen that $CaTiO_3$ was formed for sample B1 while rutile was formed for sample B5 at high temperatures. Figure 5(d) illustrates the XRD results of samples C1 and C5, respectively, which showed the similar results as samples B1 and B5. Figure 6 shows the BSE images of sample A2 quenched from 1533 K (1260 °C), and it could be seen that the crystal was typical rod-shape structure. EDX results indicated that the rod-shape crystal was TiO_2. Figure 7 shows the BSE image of sample A2 quenched from 1393 K (1120 °C), from which it could be seen that cloud- and rod-shape crystals were formed simultaneously.

From the XRD and BSE results, it can be seen that the primary crystalline phase changed from rod-shape rutile to dendrite $CaTiO_3$ with the increase of basicity, while several crystalline phases coexist with the decrease of temperature. According to ionic theory of molten slags, P_2O_5 showed the strongest acidity and its ion-oxygen parameter "I" was as high as 3.30, while the ion-oxygen parameter of SiO_2 was 2.45.[24] P_2O_5 was a typical network-forming oxide, and several kinds of anions such as PO_3^-, PO_4^{3-} and $P_2O_7^{4-}$ form in the slag melts. These anions would seriously restrict the ionic reaction between Ca^{2+} and TiO_3^{2-} to form perovskite

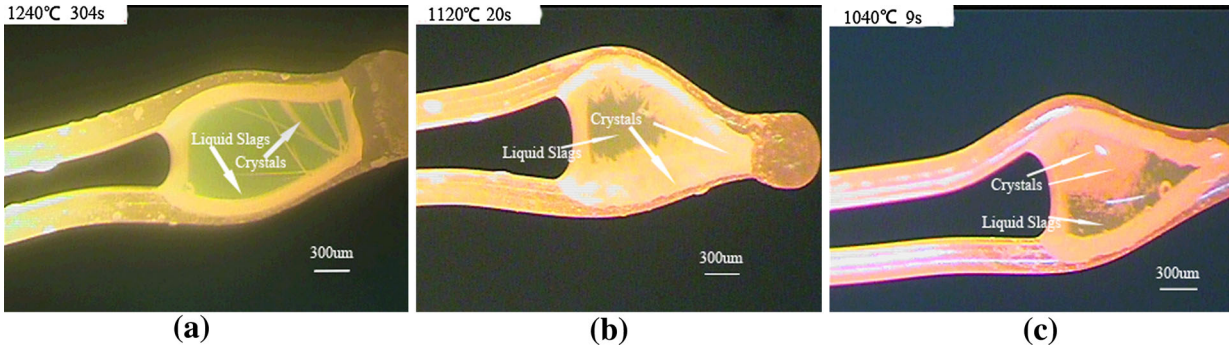

Fig. 3—Crystallization behaviors of sample A1 at (*a*) 1513 K (1240 °C), (*b*) 1393 K (1120 °C), and (*c*) 1313 K (1040 °C).

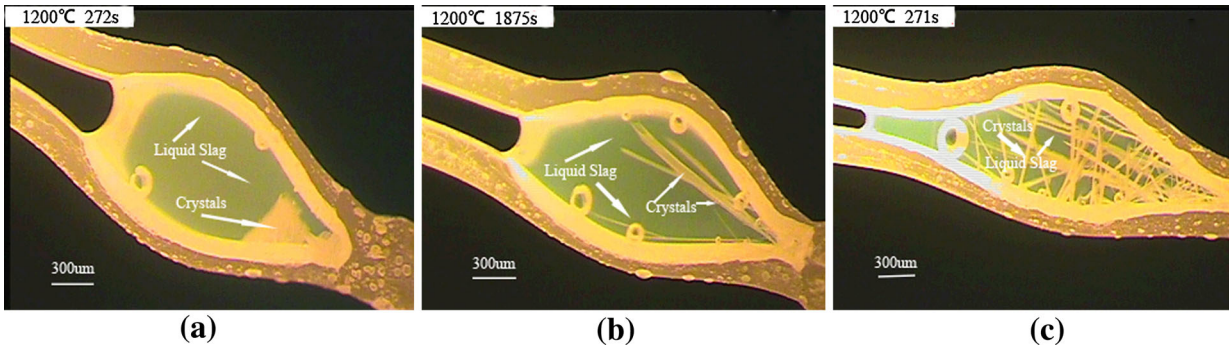

Fig. 4—Crystallization behaviors at 1473 K (1200 °C) of samples (*a*) B1, (*b*) B3, and (*c*) B5.

and, therefore, improved the crystallization trend of rutile and promoted its precipitation. To clarify the crystallization mechanism of the modified slags, the isopleth phase diagrams were calculated by Factage.[25] Figure 8 gives the isopleth phase diagrams for slags A1, B1, and C1, respectively. As can be seen from Figure 8(a), rutile was the primary phase at high temperatures for sample A1; with the decrease of temperature, the crystalline phases changed drastically, and there were always several phases coexisting, which was generally in agreement with the experimental results. From Figures 8(b) and (c), it can be seen that $CaTiO_3$ was the primary phase for samples B1 and C1, and then, $CaAl_2Si_2O_8$, $CaTiSiO_5$, and $MgSiO_3$ precipitated with the decrease of temperature. It should be noticed that there are some deviations between the phase diagrams and the experimental results, because the phase diagram was calculated in equilibrated assumption while the experiments were carried out under supercooling conditions.

C. *Kinetics of Rutile Growth*

1. *Kinetics study of crystallization process*

The kinetics of crystallization was generally studied through the Johnson–Mehl–Avrami (JMA) equation,[26–28] as shown in Eq. [1]

$$X = 1 - \exp(-k(t-\tau)^n) \qquad [1]$$

where X is the crystalline volume fraction, t is the holding time, τ is the incubation time, k is effective crystallization rate constant (including nucleation and growth), and n is the Avrami exponent associated with the nucleation and growth mechanism.

The volume fraction of crystal (X) obtained at a certain temperature was defined as:

$$X = A_c/A_T, \qquad [2]$$

where A_c is the area of crystal and A_T is the total area of sample.[20] Rearranging Eqs. [1], [3] can be obtained, and the values of k and n could be obtained by plotting $\ln(\ln(\frac{1}{1-X}))$ *vs* $\ln(t-\tau)$.

$$\ln\left(\ln\left(\frac{1}{1-X}\right)\right) = \ln k + n\ln(t-\tau) \qquad [3]$$

Arrhenius equation (shown as Eq. [4]) could be used to relate apparent crystallization rate constant (k) to temperature T, and by rearranging Eqs. [4], [5] could be obtained, through which the apparent activation energy of crystallization Ea could be determined.

$$k = A\exp\left(-\frac{E_a}{RT}\right) \qquad [4]$$

$$\ln k = \ln A - \frac{E_a}{RT}, \qquad [5]$$

where k is apparent crystallization rate constant, A is the preexponential factor, E_a is the apparent activation energy of crystallization, R is the gas constant, and T is the absolute temperature (K).

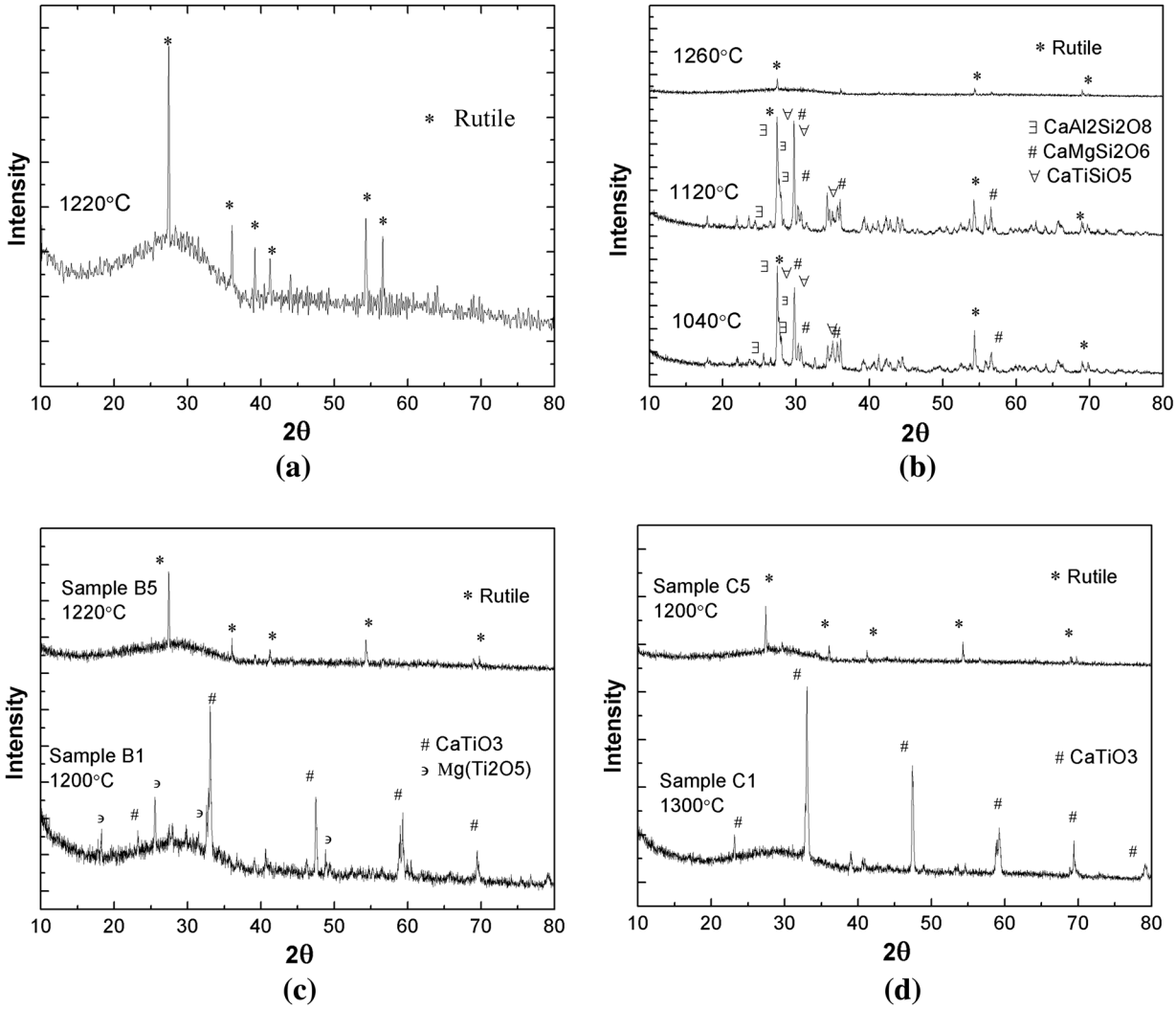

Fig. 5—XRD patterns of the quenched samples (*a*) A1 at 1493 K (1220 °C), (*b*) A2 at 1533 K (1260 °C), 1393 K (1120 °C), and 1313 K (1040 °C), (*c*) B1 at 1473 K (1200 °C) and B5 at 1493 K (1220 °C), (*d*) C1 at 1573 K (1300 °C) and C5 at 1473 K (1200 °C).

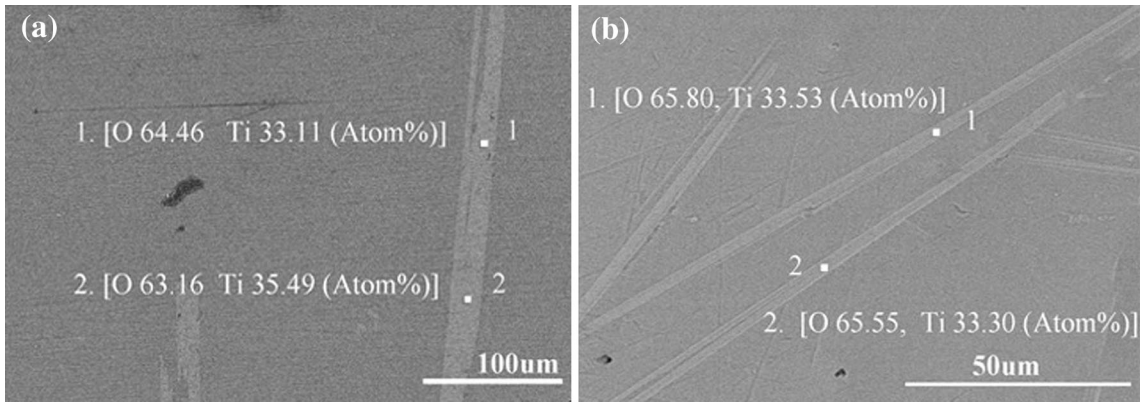

Fig. 6—BSE images of sample A2 quenched at 1533 K (1260 °C).

2. *The calculation of n and k*

The volume fraction of crystal (X) *vs* time for 9 samples that rutile can be formed was calculated under the present experiment. Figure 9 shows the calculated results of samples A1 and B3. It can be seen that $\ln(\ln(\frac{1}{1-X}))$ *vs* $\ln(t-\tau)$ shows a good linear relationship, and the n and k values were, therefore, calculated as shown in Table II. The results indicated that n value increased with decreasing

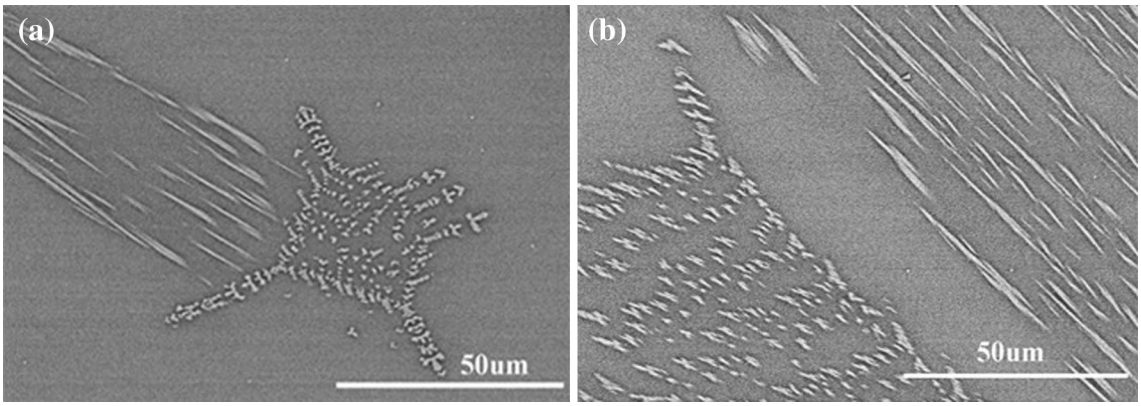

Fig. 7—BSE images of sample A2 quenched at 1393 K (1120 °C).

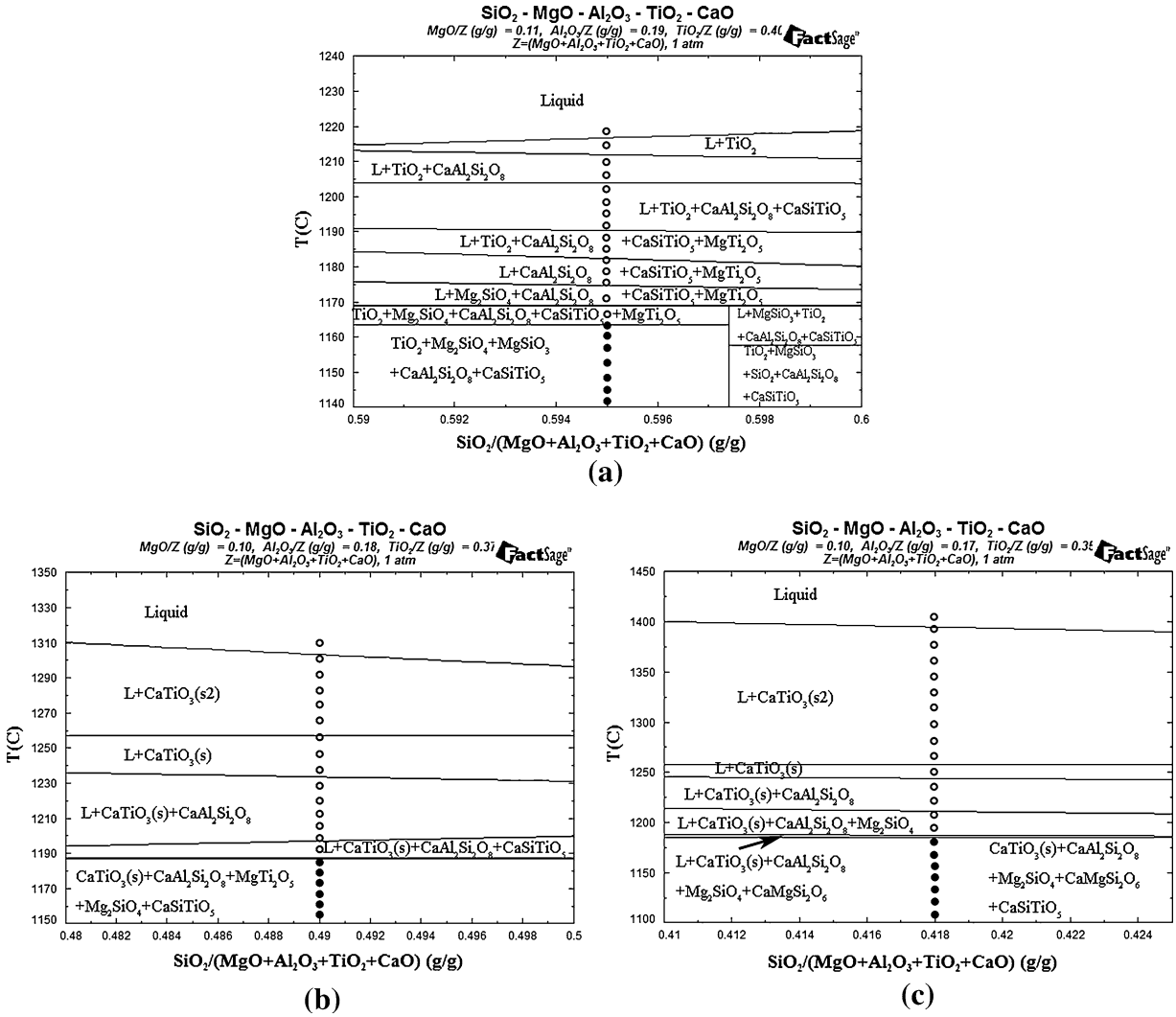

Fig. 8—Isopleths phase diagrams for samples (*a*) A1, (*b*) B1, and (*c*) C1.

temperature, which may suggest that the nucleation rate was reduced or the nucleation sites decreased.

3. *The crystallization mechanism of rutile*

According to JMA equation, the Avrami exponent n was associated with the nucleation and growth mechanism. Some researches[29–32] studied the relationship between the Avrami exponent n and the crystallization mechanism, and their relationship can be shown as follows:

$$n = a + bc, \qquad [6]$$

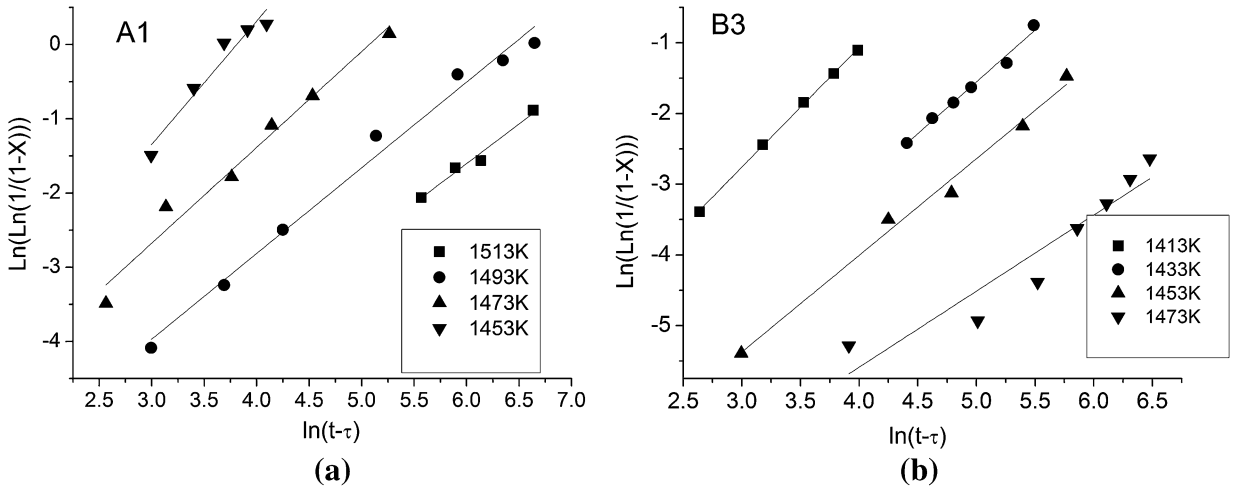

Fig. 9—Crystalline volume fraction evolution as a function of time for samples (*a*) A1 and (*b*) B3.

Table II. The Variations of *n* and *k* *vs* P_2O_5 Content and Temperature

Samples	Temperature [K (°C)]	*n*	Lnk
A1	1453 (1180)	2.35	−6.33
	1473 (1200)	1.76	−6.55
	1493 (1220)	1.15	−7.43
	1513 (1240)	0.78	−8.03
A2	1433 (1160)	1.65	−4.77
	1473 (1200)	1.27	−5.93
	1513 (1240)	1.23	−7.65
	1553 (1280)	0.94	−8.68
A3	1513 (1240)	1.75	−6.81
	1533 (1260)	1.28	−7.16
	1553 (1280)	1.29	−7.70
	1573 (1300)	0.74	−9.19
A4	1513 (1240)	2.62	−6.27
	1533 (1260)	1.74	−7.30
	1553 (1280)	1.60	−7.99
	1573 (1300)	1.35	−8.92
A5	1513 (1240)	2.51	−4.99
	1553 (1280)	1.57	−7.07
	1573 (1300)	1.54	−8.07
	1593 (1320)	1.32	−9.03
B3	1413 (1140)	1.77	−7.84
	1433 (1160)	1.77	−8.88
	1453 (1180)	1.37	−9.47
	1473 (1200)	0.90	−9.89
B4	1433 (1160)	1.67	−7.53
	1453 (1180)	1.29	−8.13
	1473 (1200)	1.23	−8.67
	1493 (1220)	1.12	−9.61
B5	1473 (1200)	1.69	−6.43
	1493 (1220)	1.52	−7.26
	1513 (1240)	1.21	−7.65
	1533 (1260)	0.97	−8.82
C5	1413 (1140)	1.37	−6.01
	1433 (1160)	1.50	−6.74
	1453 (1180)	1.31	−7.17
	1473 (1200)	1.13	−8.07

where *n* is the Avrami exponent, *a* is the constant about nucleation rate, *b* is the dimension of crystal growth, and *c* is the constant of crystal growth. The crystallization mechanism of rutile can be identified from two aspects. First, the length evolution of the rutile with time was studied according to the studies of Jackson.[30] Figure 10 shows the relation between the length evolution of the rutile and time, and it can be observed that the length *vs* time showed the linear relation, indicating that the rate-controlling step of rutile growth was interfacial reaction, which means $c = 1$. Second, the mathematical relation of these constants was studied. It is generally assumed that the rod-shape growth was one-dimensional growth, *i.e.*, $b = 1$. According to the SHTT images, nucleation rate decreased with the increase of time, *i.e.*, $0 < a < 1$; as shown in Table II, it can be seen that $1 < n < 2$ at most temperatures. Through the mathematical relation, it can be approximately concluded that *c* was about 1, *i.e.*, the reaction of the rutile growth was mainly controlled by crystal/melt interfacial reaction. This is in agreement with the first aspect. Moreover, the average growth at 1473 K (1200 °C) was obtained through the measurement of rutile length with time. The growth rates could be acquired, which was 18.81, 27.49, 6.76, and 4.15 μm/s for samples A1, A2, B4, and C5, respectively. It should be pointed out that it is hard to measure the rutile growth rate for some samples such as A3-A5 at 1473 K (1200 °C) because of the fast nucleation.

In this part, the crystallization mechanism of the rod-shape rutile was identified from two aspects and the results indicated that rutile was one-dimensional growth and the rate-controlling step was interfacial reaction.

4. *The variation of apparent crystallization activation energy*

According to Eq. [5], E_a (kJ/mol) could be determined by plotting lnk *vs* $-1000/RT$, and Figure 11(a) shows the calculation process. The plots showed obvious linear relation, and the apparent crystallization activation energy was, therefore, calculated from the slopes through Eq. [5].

Figure 11(b) shows the comparison of the calculated apparent activation energy. It can be seen that the absolute value of Ea increased with the increase of P_2O_5

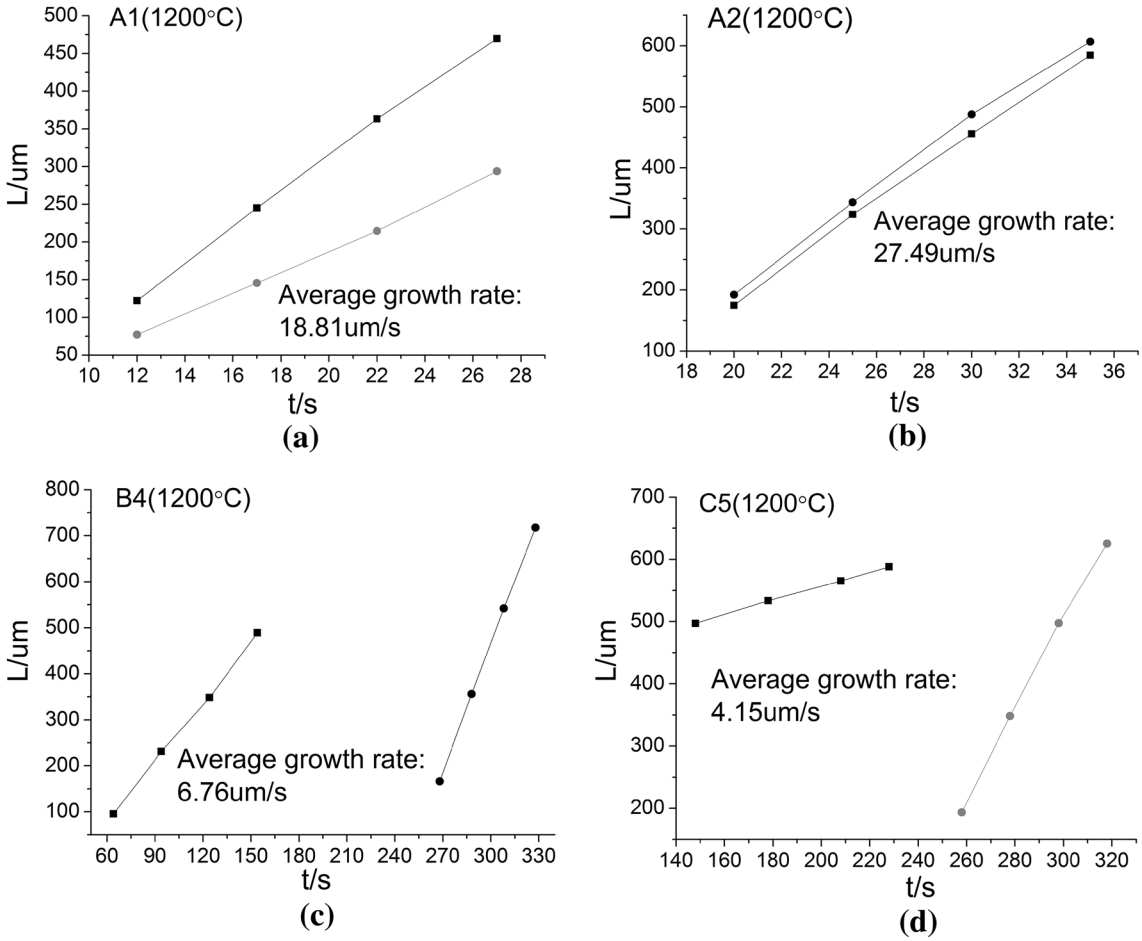

Fig. 10—Measured length evolution of rutile for different samples as a function of time.

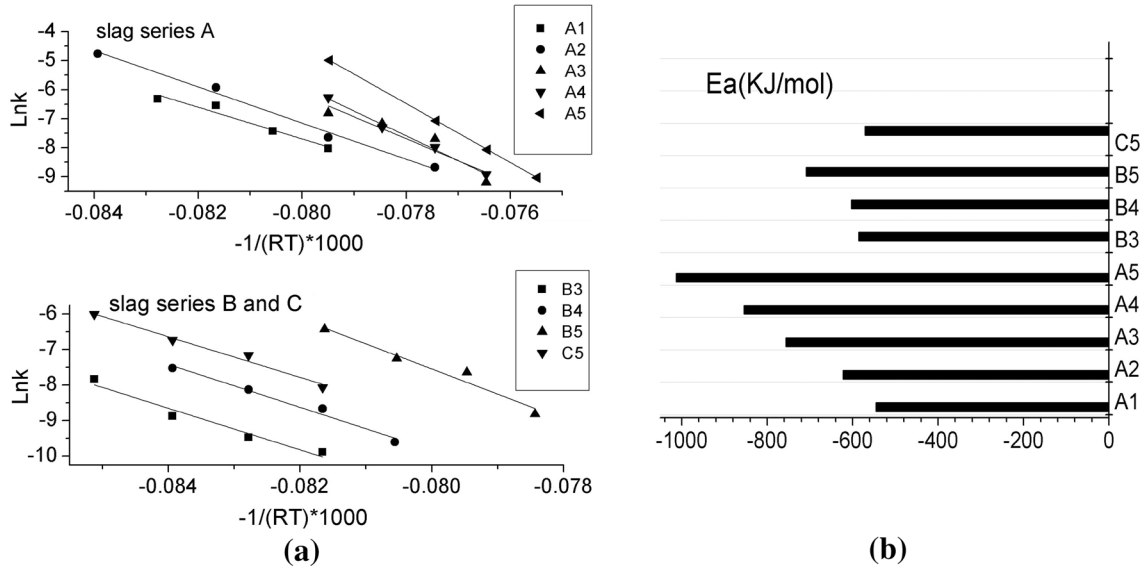

Fig. 11—Calculation of the apparent crystallization activation energy: (*a*) relation between Lnk and $-1000/RT$, (*b*) change of the activation energy.

content, while it decreased with increasing basicity. According to Eq. [4], it could be concluded that the higher P_2O_5 content enhanced the precipitation of the rod-shape crystal, while the higher basicity suppressed the growth of the rod-shape crystal. This is consistent with the aforementioned TTT results.

IV. CONCLUSIONS

In the present experiments, the effect of basicity and P_2O_5 on the crystallization behaviors of Ti-bearing blast furnace slags was investigated using SHTT and TTT diagrams were, therefore, constructed. It was found that the trend of rutile formation decreased with increasing basicity, and the crystallization of rutile was promoted by the addition of P_2O_5. With the increase of P_2O_5 content, the basicity and the crystallization temperature at which the rod-shape rutile was precipitated became higher. Rutile showed the rod-shape structure, and the crystallization was one-dimensional interface-controlled growth. The absolute value of the apparent activation energy increased with the increase of P_2O_5 content.

ACKNOWLEDGMENTS

The authors gratefully acknowledge financial support by the Common Development Fund of Beijing and the National Natural Science Foundation of China (51172001, 51074009, and 51172003). Supports by the National High Technology Research and Development Program of China (863 Program, 2012AA06A114) and Key Projects in the National Science & Technology Pillar Program (2011BAB03B02 and 2011BAB02B05) are also acknowledged.

REFERENCES

1. L.P. Wang, H. Wang, G. Qi, X.J. Li, Z.Q. Chen, and Y.Q. Dou: *Chin. J. Rare Met*., 2004, vol. 28 (1), pp. 265–67.
2. J. Li, Z.T. Zhang, M. Zhang, M. Guo, and X.D. Wang: *Steel Res. Int*., 2011, vol. 82 (6), pp. 607–14.
3. L. Wen and J.Z. Zhang: *J. Iron Steel Res.*, 2011, vol. 23 (5), pp. 1–3, 19.
4. F. Yan, C. Li, and B. Liang: *Chin. J. Process Eng*., 2006, vol. 6 (3), pp. 413–17.
5. X.H. Liu and Z.T. Sui: *Chin. J. Nonferrous Met*., 2002, vol. 12 (6), pp. 1281–84.
6. Z.M. Zhou, B.H. Zhang, and Z.Z. Zhu: *Iron Steel Vanadium Titan*., 1999, vol. 20 (4), pp. 35–38.
7. K. Sun, J.H. Wu, and Y.Y. Ma: *Iron Steel Vanadium Titan*., 2000, vol. 21 (3), pp. 54–58.
8. Y. Peng: *Titan. Ind. Prog*., 2005, vol. 22 (6), pp. 45–49.
9. S.H. Huang, J.Y. Pan, and R.L. Zhang: *Iron Steel Vanadium Titan*., 1994, vol. 15 (2), pp. 17–21.
10. M.Y. Wang, L.N. Zhang, L. Zhang, Z.T. Sui, and G.F. Tu: *Trans. Nonferrous Met. Soc. China*, 2006, vol. 16 (2), pp. 421–25.
11. Y.H. Li, T.P. Lou, and Z.T. Sui: *Chin. J. Nonferrous Met*., 2000, vol. 10 (5), pp. 719–722.
12. P.M. Guo and P. Zhao: *Iron Steel Vanadium Titan*., 2005, vol. 26 (2), pp. 5–10.
13. J. Li, Z.T. Zhang, and X.D. Wang: *ISIJ Int*., 2011, vol. 51 (9), pp. 1396–402.
14. J. Li, Z.T. Zhang, and X.D. Wang: *Ironmak. Steelmak*., 2012, vol. 39 (6), pp. 414–18.
15. J Li, XD Wang, and ZT Zhang: *ISIJ Int*, 2013, vol. 53 (10), pp. 1696–703.
16. Y. Kashiwaya, C.E. Cicutti, A.W. Cramb, and K. Ishii: *ISIJ Int*., 1998, vol. 38 (4), pp. 348–56.
17. Y. Kashiwaya, C.E. Cicutti, and A.W. Cramb: *ISIJ Int*., 1998, vol. 38 (4), pp. 357–65.
18. Z.T. Zhang, J. Li, and P. Liu: *J. Iron. Steel Res. Int*., 2011, vol. 18 (5), pp. 31–37.
19. Z.T. Zhang, G. Wen, and Y.Y. Zhang: *Int. J. Miner. Metall. Mater*., 2011, vol. 18 (2), pp. 150–58.
20. L.J. Zhou, W.L. Wang, F.J. Ma, J. Li, J. Wei, H. Matsuura, and F. Tsukihashi: *Metall. Mater. Trans. B*, 2012, vol. 43B, pp. 354–62.
21. H.G. Ryu, Z.T. Zhang, J.W. Cho, and S. Sridhar: *ISIJ Int*., 2010, vol. 50 (8), pp. 1142–50.
22. J. Li, W.L. Wang, J. Wei, and H. Matsuura: *ISIJ Int*., 2012, vol. 52 (12), pp. 2220–25.
23. H. SuiTo and R. Inoue: *ISIJ Int*., 2006, vol. 46 (2), pp. 180–87.
24. Y. Waseda and J.M. Toguri: *The Structure and Properties of Oxide Melts*, World Scientific Publishing, Singapore, 2002, p. 189.
25. C.W. Bale, P. Chartrand, S.A. Degterov, G. Eriksson, K. Hack, R. Ben Mahfoud, J. Melancon, A.D. Pelton, and S. Peterson: *CALPHAD*, 2002, vol. 26 (2), pp. 189–228.
26. M.C. Weinberg, D.P. Birnie, III, and V.A. Shneidman: *J. Non-Cryst. Solids*, 1997, vol. 219, pp. 89–99.
27. D.A. Porter and K.E. Eastering: *Phase Transformations in Metals and Alloys*, 2nd ed., CRC Press, New York, NY, 2004, pp. 287–90.
28. A. Marotta and A. Buri: *J. Mater. Sci*., 1981, vol. 16 (2), pp. 341–44.
29. S. Ranganathan and M. Vonheimendahl: *J. Mater. Sci*., 1981, vol. 16 (9), pp. 2401–04.
30. K.A. Jackson: *Liquid Metals and Solidification*, ASM, Cleveland, OH, 1958, p. 174.
31. G. Ruitenberg, E. Woldt, and A.K. Petford-Long: *Thermochim. Acta*, 2001, vol. 378 (1), pp. 97–105.
32. J. Huberty and H.F. Xu: *J. Solid State Chem*., 2008, vol. 181 (3), pp. 508–14.